Arch Appl Mech (2014) 84:967–983
DOI 10.1007/s00419-014-0842-1

ORIGINAL

G. Falsone · D. Settineri · I. Elishakoff

A new locking-free finite element method based on more consistent version of Mindlin plate equation

Received: 1 August 2013 / Accepted: 5 March 2014 / Published online: 26 March 2014

Abstract A finite element (FE) approach is presented for the dynamic analysis of the Mindlin plates considering both shear deformation and rotary inertia effects. The model is based on the consistent version of the Mindlin equations, which neglects the higher-order time derivative contribution. The approach provides a new class of interdependent Hermite shape polynomials by the definition of a fictitious deflection that takes into account the effective interdependence between the generalized displacements in both the continuous and FE discretized schemes. This implies that the proposed approach is free-shear-locking and is characterized by a good accuracy even for low-order FEs. Several examples are considered whose results are compared with analogous ones proposed in the literature with other approaches.

Keywords Fictitious displacement · Shear deformation · Rotary inertia · FEM · Mindlin plate

1 Introduction

In the technical theory of the bending plates, two of the most used models are the well-known Kirchhoff plate model (KPM) and Mindlin plate model (MPM). One of the most relevant problems in the application of the finite element (FE) methods to the MPM is the so-called shear-locking phenomenon that arises due to the impossibility of reproducing the pure bending modes in the limit case of thin plates and for the consequent inclusion of zero shear strain constraints in the variational formulation of the problem [1,2]. This is essentially due to the impossibility of reproducing correctly the interdependence among the deflection and the two rotations by the FE schemes. In order to overcome this problem, without increasing the order of the FEs with the consequent computational cost increasing, many approaches have been presented in the literature. For quadrilateral FEs, a class of approaches proposes the use of the same order polynomials for interpolating both the deflection and the two rotations and of a reduced integration scheme for the shear term [3–5]. However, in some cases, the shear-locking is not resolved by these procedures and in other cases, some problems of artificial zero-energy modes arise. Another relevant class of methods is based on the mixed formulation of hybrid FEs [6–8]. Unfortunately, the corresponding formulations are complex and the computational cost is high. The assumed natural strain (ANS) method is developed to eliminate the shear-locking for bilinear plate FEs [9]. Its basic idea lies on the computation of the shear strains at discrete collocation points from the displacements. Afterward, they are interpolated over the element with specific shape functions. Many ANS versions of plate and shell FEs have been developed, and an overview can be found in some textbooks [10,11]. A methodology, which

G. Falsone · D. Settineri (✉)
Dipartimento di Ingegneria Civile, Informatica, Edile, Ambientale e Matematica Applicata, Università di Messina, C.da Di Dio, 98166 Messina, Italy
E-mail: dsettineri@unime.it

I. Elishakoff
Department of Mechanical Engineering, Florida Atlantic University, Boca Raton, FL 33431-0991, USA

can be considered similar to the ANS approach, is the discrete shear gap (DSG) method [12], in the sense that the course of certain strains is modified within the FE, too. The main difference consists in the lack of collocation points making application of the DSG independent of the order and form of the FEs. Recently, the DSG method has been extensively used as coupled with the so-called Edge-based Smoothed FE Method (ES-FEM) [13] that is a particular mesh-free FE approach [14].

More recently, Falsone and Settineri [15] have proposed a free-locking element based on a new class of interdependent shape polynomials that take into account the exact interdependence between the kinematic variables; as a consequence, the model is able to reproduce the pure bending mode in the limit case of thin plate. This model was proposed for the static problem of the MPM and, in general, must be modified for the dynamic analysis; as a matter of fact, the new method proposed by the authors—first introduced for the static problem of the Timoshenko beam [16]—is based on the derivation of the exact interdependent shape polynomials that in turn are strictly related to the differential problem. This problem in the dynamic study must consider the translatory and rotary inertia terms that appear in the equilibrium equations. Considering both shear deformation and rotary inertia effects, higher-order time derivative contributions are involved in the solution of the plate. This problem was studied by several authors to investigate the contribution of these terms that appear both in the Timoshenko beam and the Mindlin plate. Stephen [17,18], proposing a study of the second spectrum of the Timoshenko beam, affirms that second spectrum is "an inevitable but meaningless consequence of the structures of an otherwise excellent approximate theory," remarking this position in another work [19] dealing the validity of the Mindlin higher-order spectra. Here, the author dismissed one of two higher spectra while Levinson [20] dismissed the second one. Remarkably, Elishakoff [21] arrived at the conclusion that the higher-order time derivative effect must be neglected, that is, the higher-order time derivative must not appear in the equilibrium equations. As a consequence, the consequent differential problem becomes simpler and the related problem is more consistent than the original one.

In this paper, a new FE approach is proposed for the dynamic analysis of the Mindlin plate. This work has two aims such as (1) to extend the free-locking FE approach obtained for the static case to the dynamic problem, both considering the shear and rotary inertia effects; (2) to provide a FE formulation that neglects the higher-order time derivative effect. In particular, to perform the second aim, the simpler and more consistent version of the Mindlin equations will be used. The new method is based on the introduction of a new generalized variable for the dynamic problem, that is, the fictitious deflection, whose advantageous and inherent aspects will be extensively treated in the paper.

2 Preliminary concepts

In order to make clear the symbols used in the following, in this section, the relationships governing the MPM dynamic behavior will be briefly shown. Moreover, in order to simplify the form of the relationships, the dependence of the static and kinematic quantities on the spatial and temporal variables will be considered implicitly.

Considering a Cartesian reference $(O; x, y, z)$, with the z axis orthogonal to the plate mid-plane, the behavior of the plate is defined by the knowledge of the generalized kinematic variables that are the deflection along the z axis and the rotations around the axes x and y, respectively, indicated by w, φ_y and φ_x. These quantities are related each other by the following compatibility equations:

$$\gamma_x = \varphi_x + \frac{\partial w}{\partial x}; \quad \gamma_y = \varphi_y + \frac{\partial w}{\partial y} \tag{1a,b}$$

where γ_x and γ_y are the generalized shear angle strains.

Under the assumption of elastic isotropic material, the static fundamental quantities of the plate are defined by the following differential relationships:

$$M_x = D\left(\frac{\partial \varphi_x}{\partial x} + \nu \frac{\partial \varphi_y}{\partial y}\right); \quad M_y = D\left(\frac{\partial \varphi_y}{\partial y} + \nu \frac{\partial \varphi_x}{\partial x}\right); \quad M_{xy} = \frac{1}{2}\hat{D}\left(\frac{\partial \varphi_x}{\partial y} + \frac{\partial \varphi_y}{\partial x}\right)$$
$$Q_x = S\left(\varphi_x + \frac{\partial w}{\partial x}\right); \quad Q_y = S\left(\varphi_y + \frac{\partial w}{\partial y}\right) \tag{2a–e}$$

where M_x and M_y are the generalized bending moments acting around the axis y and x, respectively; M_{xy} is the twisting moment, and Q_x and Q_y are the generalized shear forces acting on the sections having the

axes x and y as normal vectors, respectively. Into Eqs. (2), the quantities D, $\hat{D}$ and S characterize the stiffness proprieties of the plate and are given by the following relationships:

$$D = \frac{Eh^3}{12\left(1-\nu^2\right)}; \quad \hat{D} = \frac{Gh^3}{6}; \quad S = \chi Gh \tag{3a–c}$$

where E and G are the material Young's modulus and shear modulus, respectively; ν is the Poisson ratio; h is the plate thickness; and χ is the shear factor. Moreover, the stiffness parameters D and $\hat{D}$ can be related by the following relation, which will be useful in the next sections:

$$D = \nu D + \hat{D} \tag{4}$$

The dynamic equilibrium equations governing the free vibrations of the plate assume the following form:

$$\frac{\partial M_x}{\partial x} + \frac{\partial M_{xy}}{\partial y} = Q_x + r_I \frac{\partial^2 \varphi_x}{\partial t^2}; \quad \frac{\partial M_{xy}}{\partial x} + \frac{\partial M_y}{\partial y} = Q_y + r_I \frac{\partial^2 \varphi_y}{\partial t^2};$$
$$\frac{\partial Q_x}{\partial x} + \frac{\partial Q_y}{\partial y} = r_A \frac{\partial^2 w}{\partial t^2} \tag{5a–c}$$

where $r_I = \rho h^3/12$ and $r_A = \rho h$ are the rotary and translatory inertia, respectively, ρ being the material density. Substituting the expression of the shear forces from Eq. (5a-b) into Eq. (5c) and using Eqs. (2a-c) to obtain the bending and twisting moment in terms of the generalized rotations, by simple algebra, the following relationship is obtained:

$$D\nabla^2\left(\frac{\partial \varphi_x}{\partial x} + \frac{\partial \varphi_y}{\partial y}\right) = r_A \frac{\partial^2 w}{\partial t^2} + r_I \frac{\partial^2}{\partial t^2}\left(\frac{\partial \varphi_x}{\partial x} + \frac{\partial \varphi_y}{\partial y}\right) \tag{6}$$

where $\nabla^2(\bullet)$ is the Laplace operator. Using the compatibility equations given in Eqs. (1), together with the equilibrium equation given in Eq. (5c) and the constitutive equations given in Eqs. (2d-e), the quantity into parentheses in Eq. (6) can be rewritten as follows:

$$\frac{\partial \varphi_x}{\partial x} + \frac{\partial \varphi_y}{\partial y} = \frac{r_A}{S}\frac{\partial^2 w}{\partial t^2} - \nabla^2 w \tag{7}$$

Substituting the above relationship in Eq. (6) and collecting the common terms, the equation governing the free vibrations of a Mindlin plate is obtained in the form:

$$\nabla^4 w - \left(\frac{r_A}{S} + \frac{r_I}{D}\right)\frac{\partial^2 \nabla^2 w}{\partial t^2} + \frac{r_A}{D}\frac{\partial^2 w}{\partial t^2} + \frac{r_A}{S}\frac{r_I}{D}\frac{\partial^4 w}{\partial t^4} = 0 \tag{8}$$

Equation (8) shows that the simultaneous effects of the shear deformation and rotary inertia provide an higher-order time derivative contribution, that is, the last term appearing in the equation. In this paper, a simplified version of this equation will be used by deleting this term, with the final purpose to define a new free-locking finite element model for the Mindlin plate able to takes into account both the shear deformation and the rotary inertia effects without unphysical results in terms of response spectra.

3 The simpler and more consistent version of the Mindlin equation

Equation (8) can be considered as a generalization to the plate case of the Bresse–Timoshenko equation. The Bresse–Timoshenko equation has been studied by several authors with the aim to investigate the known anomaly that the Timoshenko beam exhibits if the simultaneous effects of shear deformation and rotary inertia are considered. As a matter of fact, it is well known that in this case, the Timoshenko beam is associated with two frequency spectra, the second of which is considered unphysical by several authors [17,18,21,22]. Stephen [18] focuses the aspect that this anomaly is due to the higher-order time derivative contribution. Already, Timoshenko [23] in 1921 notices that the fourth-order derivative term changes natural frequencies insignificantly. Elishakoff [21] demonstrated that the "simplified" equation was more consistent and simpler

than the original Bresse–Timoshenko one. In fact, neglecting the term linked to the fourth-order time derivative, one obtains a simpler equation that is associated only to the first frequency spectrum.

Hence, the term related to the fourth-order time derivative appearing in Eq. (8) can be interpreted as a higher-order correction term of the KPM, which is related to the inertia contribution. Based on this consideration, a simplified version of the Mindlin plate equation can be obtained by considering the following equilibrium equation instead of that given in Eqs. (5a–b):

$$\frac{\partial M_x}{\partial x}+\frac{\partial M_{xy}}{\partial y}=Q_x-r_I\frac{\partial^3 w}{\partial t^2\partial x};\quad \frac{\partial M_{xy}}{\partial x}+\frac{\partial M_y}{\partial y}=Q_y-r_I\frac{\partial^3 w}{\partial t^2\partial y}; \tag{9a,b}$$

This means that the rotary effects taken into account in the equilibrium equation are the same considered in the KPM. Using these equations, it is not difficult to verify that Eq. (6) can be rewritten as follows:

$$D\nabla^2\left(\frac{\partial\varphi_x}{\partial x}+\frac{\partial\varphi_y}{\partial y}\right)=r_A\frac{\partial^2 w}{\partial t^2}-r_I\frac{\partial^2}{\partial t^2}\nabla^2 w \tag{10}$$

Then, using Eq. (7), the simplified Mindlin equation for the dynamic problem is obtained:

$$\nabla^4 w-\left(\frac{r_I}{D}+\frac{r_A}{S}\right)\nabla^2\frac{\partial^2 w}{\partial t^2}+\frac{r_A}{D}\frac{\partial^2 w}{\partial t^2}=0 \tag{11}$$

This equation differs from the complete one given in Eq. (8) only for the absence of the fourth-order time derivative contribution. It is the generalization of the "simplified" version of the Bresse–Timoshenko equation proposed by Elishakoff [22]. Thus, Eq. (11) is both simpler and more consistent than the original Mindlin equation. Elishakoff [24] pointed out that the original Mindlin theory is inconsistent in the sense that it takes into account secondary effect of the interaction between the shear deformation and rotary inertia. Likewise, it should be noted that Eq. (11) was established as a rigorous approximation in [25].

Even if in the present work Eq. (11) will be no more used; nevertheless, the modified version of the equilibrium equation given into Eqs. (9) will be advantageously considered in the next section.

4 The fictitious deflection in the Mindlin plate dynamic problem

With the aim of proposing an innovative finite element model for the static problem of the Timoshenko beam, in [16], a new kinematic variable was introduced for the solution of the elastic problem; this variable was defined "fictitious deflection" and indicated as $\bar{w}$. This variable has the propriety of being able to define the full solution of the equilibrium elastic problem and, in the case of slender beam, it coincides with the deflection itself. Subsequently, the same authors have extended the concept of fictitious deflection to the static problem of the MPM [15]. The fictitious deflection, in addition to defining the static problem of the plate and of the beam in a more convenient form, has the advantage of incorporating the effects of shear deformation. Therefore, the problem reformulated in light of its use has the mathematical structure of the corresponding slender elements.

In the dynamic problem, the fictitious deflection acquires a broader meaning since it encompasses not only the effect of the shear deformability but also the rotary inertia effect. Here, the fictitious deflection is introduced for the dynamic problem of the simplified and consistent version of the MPM defined in the previous section. As a consequence, the advantages concerning in its use will be shown and discussed.

The fictitious deflection $\bar{w}$ is defined in such a way that it satisfies the following integral–differential equations:

$$\int\varphi_x\mathrm{d}x=-\bar{w}+\frac{r_I}{r_A}\nabla^2\bar{w}+f_x;\quad \int\varphi_y dy=-\bar{w}+\frac{r_I}{r_A}\nabla^2\bar{w}+f_y \tag{12a,b}$$

where $f_x=f_x(t,y)$ and $f_y=f_y(t,x)$ are arbitrary functions of which the first does not depend on x and the second does not depend on y. By differentiating Eq. (12a) with respect to x and Eq. (12b) with respect to y, one obtains the following relationships for the rotations:

$$\varphi_x=-\frac{\partial\bar{w}}{\partial x}+\frac{r_I}{r_A}\frac{\partial\nabla^2\bar{w}}{\partial x};\quad \varphi_y=-\frac{\partial\bar{w}}{\partial y}+\frac{r_I}{r_A}\frac{\partial\nabla^2\bar{w}}{\partial y} \tag{13a,b}$$

Then, from Eqs. (2a–c), the bending and twisting moments become

$$M_x = -D\left(\frac{\partial^2 \bar{w}}{\partial x^2} + \nu \frac{\partial^2 \bar{w}}{\partial y^2}\right) + \frac{r_I}{r_A} D\left(\frac{\partial^2 \nabla^2 \bar{w}}{\partial x^2} + \nu \frac{\partial^2 \nabla^2 \bar{w}}{\partial y^2}\right);$$
$$M_y = -D\left(\frac{\partial^2 \bar{w}}{\partial y^2} + \nu \frac{\partial^2 \bar{w}}{\partial x^2}\right) + \frac{r_I}{r_A} D\left(\frac{\partial^2 \nabla^2 \bar{w}}{\partial y^2} + \nu \frac{\partial^2 \nabla^2 \bar{w}}{\partial x^2}\right);$$
$$M_{xy} = -\hat{D}\frac{\partial^2 \bar{w}}{\partial x \partial y} + \hat{D}\frac{r_I}{r_A}\frac{\partial^2 \nabla^2 \bar{w}}{\partial x \partial y} \tag{14a–c}$$

In order to obtain the expression of the shear forces, the rotational equilibrium equations given in Eqs. (5a,b) can be modified by substituting the expression of the second-order time derivative of the deflection obtained from the translational equilibrium equation given in Eq. (5c) and then, using also Eqs. (14), one obtains the following equalities:

$$-D\left(\frac{\partial^3 \bar{w}}{\partial x^3} + \nu \frac{\partial^3 \bar{w}}{\partial y^2 \partial x}\right) + \frac{r_I}{r_A} D\left(\frac{\partial^3 \nabla^2 \bar{w}}{\partial x^3} + \nu \frac{\partial^3 \nabla^2 \bar{w}}{\partial y^2 \partial x}\right) - \hat{D}\frac{\partial^3 \bar{w}}{\partial x \partial y^2}$$
$$+\hat{D}\frac{r_I}{r_A}\frac{\partial^3 \nabla^2 \bar{w}}{\partial x \partial y^2} = Q_x - \frac{r_I}{r_A}\left(\frac{\partial^2 Q_x}{\partial x^2} + \frac{\partial^2 Q_y}{\partial y \partial x}\right);$$
$$-\hat{D}\frac{\partial^3 \bar{w}}{\partial x^2 \partial y} + \hat{D}\frac{r_I}{r_A}\frac{\partial^3 \nabla^2 \bar{w}}{\partial x^2 \partial y} - D\left(\frac{\partial^3 \bar{w}}{\partial y^3} + \nu \frac{\partial^3 \bar{w}}{\partial x^2 \partial y}\right) + \frac{r_I}{r_A} D\left(\frac{\partial^3 \nabla^2 \bar{w}}{\partial y^3} + \nu \frac{\partial^3 \nabla^2 \bar{w}}{\partial x^2 \partial y}\right)$$
$$= Q_y - \frac{r_I}{r_A}\left(\frac{\partial^2 Q_y}{\partial y^2} + \frac{\partial^2 Q_x}{\partial y \partial x}\right); \tag{15a,b}$$

Regrouping these equations, also taking into account Eq. (4), simple algebra gives

$$-D\left(\frac{\partial^3 \bar{w}}{\partial x^3} + \frac{\partial^3 \bar{w}}{\partial y^2 \partial x}\right) + \frac{r_I}{r_A} D\left(\frac{\partial^3 \nabla^2 \bar{w}}{\partial x^3} + \frac{\partial^3 \nabla^2 \bar{w}}{\partial y^2 \partial x}\right) = Q_x - \frac{r_I}{r_A}\left(\frac{\partial^2 Q_x}{\partial x^2} + \frac{\partial^2 Q_y}{\partial y \partial x}\right);$$
$$-D\left(\frac{\partial^3 \bar{w}}{\partial y^3} + \frac{\partial^3 \bar{w}}{\partial x^2 \partial y}\right) + \frac{r_I}{r_A} D\left(\frac{\partial^3 \nabla^2 \bar{w}}{\partial y^3} + \frac{\partial^3 \nabla^2 \bar{w}}{\partial x^2 \partial y}\right) = Q_y - \frac{r_I}{r_A}\left(\frac{\partial^2 Q_y}{\partial y^2} + \frac{\partial^2 Q_x}{\partial y \partial x}\right); \tag{16a,b}$$

By explicating the Laplace operator, the above equalities can be rewritten as follows:

$$-D\left(\frac{\partial^3 \bar{w}}{\partial x^3} + \frac{\partial^3 \bar{w}}{\partial y^2 \partial x}\right) + \frac{r_I}{r_A} D\left(\frac{\partial^5 \bar{w}}{\partial x^5} + \frac{\partial^5 \bar{w}}{\partial y^2 \partial x^3}\right)$$
$$+\frac{r_I}{r_A} D\left(\frac{\partial^5 \bar{w}}{\partial x^3 \partial y^2} + \frac{\partial^5 \bar{w}}{\partial y^4 \partial x}\right) = Q_x - \frac{r_I}{r_A}\left(\frac{\partial^2 Q_x}{\partial x^2} + \frac{\partial^2 Q_y}{\partial y \partial x}\right);$$
$$-D\left(\frac{\partial^3 \bar{w}}{\partial y^3} + \frac{\partial^3 \bar{w}}{\partial x^2 \partial y}\right) + \frac{r_I}{r_A} D\left(\frac{\partial^5 \bar{w}}{\partial y^5} + \frac{\partial^5 \bar{w}}{\partial x^2 \partial y^3}\right)$$
$$+\frac{r_I}{r_A} D\left(\frac{\partial^5 \bar{w}}{\partial y^3 \partial x^2} + \frac{\partial^5 \bar{w}}{\partial x^4 \partial y}\right) = Q_y - \frac{r_I}{r_A}\left(\frac{\partial^2 Q_y}{\partial y^2} + \frac{\partial^2 Q_x}{\partial y \partial x}\right); \tag{17a–b}$$

From Eqs. (17), it is easy to verify that the shear forces have the following expressions:

$$Q_x = -D\left(\frac{\partial^3 \bar{w}}{\partial x^3} + \frac{\partial^3 \bar{w}}{\partial y^2 \partial x}\right) = -D\frac{\partial \nabla^2 \bar{w}}{\partial x}; \quad Q_y = -D\left(\frac{\partial^3 \bar{w}}{\partial y^3} + \frac{\partial^3 \bar{w}}{\partial x^2 \partial y}\right) = -D\frac{\partial \nabla^2 \bar{w}}{\partial y} \tag{18a–b}$$

Equations (18) and (14) are the expressions of the static quantities in terms of the fictitious deflection $\bar{w}$, while Eqs. (13) define the expression of the generalized rotation in terms of $\bar{w}$.

Let us show that $\bar{w}$ satisfies simultaneously the integral–differential equations given into Eqs. (12); this means that if the fictitious deflection exists, the Eqs. (13) must provide the same expression for the deflection. By integrating Eqs. (1) and taking into account the constitutive equations given in Eqs. (2d–e), one obtains

$$w = -\int \varphi_x \mathrm{d}x + \frac{1}{S}\int Q_x \mathrm{d}x + g_x; \quad w = -\int \varphi_y \mathrm{d}y + \frac{1}{S}\int Q_y \mathrm{d}y + g_y \tag{19a–b}$$

where $g_x = g_x(y,t)$ and $g_y = g_y(x,t)$ are integrating functions. Using Eqs. (13) and (18) and setting $f_x = g_x$ and $f_y = g_y$, after simple algebra, the following equalities are obtained

$$w = \bar{w} - \frac{r_I}{r_A}\nabla^2\bar{w} - \frac{D}{S}\nabla^2\bar{w}; \quad w = \bar{w} - \frac{r_I}{r_A}\nabla^2\bar{w} - \frac{D}{S}\nabla^2\bar{w}, \tag{20a–b}$$

that is, the Eqs. (13) provide the same expression for the deflection:

$$w = \bar{w} - \left(\frac{r_I}{r_A} + \frac{D}{S}\right)\nabla^2\bar{w} \tag{21}$$

At last, the kinematic variables are related to the fictitious deflection by the following relationships:

$$w = \bar{w} - \left(\frac{r_I}{r_A} + \frac{D}{S}\right)\nabla^2\bar{w}; \quad \varphi_x = -\frac{\partial\bar{w}}{\partial x} + \frac{r_I}{r_A}\frac{\partial\nabla^2\bar{w}}{\partial x}; \quad \varphi_y = -\frac{\partial\bar{w}}{\partial y} + \frac{r_I}{r_A}\frac{\partial\nabla^2\bar{w}}{\partial y} \tag{22a–c}$$

These equations will prove to be advantageously used in the next section.

Lastly, the single governing equation can be obtained from Eq. (5c) by substituting Eqs. (18) and (21) in it:

$$\nabla^4\bar{w} - \left(\frac{r_I}{D} + \frac{r_A}{S}\right)\frac{\partial^2\nabla^2\bar{w}}{\partial t^2} + \frac{r_A}{D}\frac{\partial^2\bar{w}}{\partial t^2} = 0 \tag{23}$$

This equation is quite analogous to that showed in Eq. (11) for the Mindlin plate; this means that the single governing equation expressed in terms of deflection or fictitious deflection does not change. However, the boundary conditions change because they are defined by Eqs. (13), (14), (18), and (21).

In order to study the free vibrations of the plate, the fictitious deflection can be expressed as $\bar{w} = \bar{U}\mathrm{e}^{i\omega t}$, where $\bar{U} = \bar{U}(x,y)$ is the eigenfunction. Using this relation in Eqs. (22), the eigenfunctions for the kinematic variables are obtained in the following form:

$$\begin{aligned} &w = U\mathrm{e}^{i\omega t}; \quad U = \bar{U} - \left(\frac{r_I}{r_A} + \frac{D}{S}\right)\nabla^2\bar{U};\\ &\varphi_x = \Phi_x\mathrm{e}^{i\omega t}; \quad \Phi_x = -\frac{\partial\bar{U}}{\partial x} + \frac{r_I}{r_A}\frac{\partial\nabla^2\bar{U}}{\partial x};\\ &\varphi_y = \Phi_y\mathrm{e}^{i\omega t}; \quad \Phi_y = -\frac{\partial\bar{U}}{\partial y} + \frac{r_I}{r_A}\frac{\partial\nabla^2\bar{U}}{\partial y} \end{aligned} \tag{24a–f}$$

where $\Phi_x = \Phi_x(x,y)$, $\Phi_y = \Phi_y(x,y)$ and $U = U(x,y)$ are the eigenfunctions of the rotations and the deflection, respectively. Equations (24) will be used in next section in order to derive a new class of interdependent Hermite shape polynomials for the MPM.

5 The interdependent shape polynomials for the Mindlin plate model

The new finite element model is obtained by assuming a polynomial approximation for the eigenfunction of the fictitious deflection $\bar{w}$ as follows:

$$\bar{U} \approx \boldsymbol{\psi}^T\bar{\mathbf{u}} = \sum_{j=1}^{r}\psi_j\bar{u}_j; \quad \boldsymbol{\psi}^T = (\psi_1 \quad \psi_2 \quad \cdots \quad \psi_r); \quad \bar{\mathbf{u}}^T = (\bar{u}_1 \quad \bar{u}_2 \quad \cdots \quad \bar{u}_r) \tag{25a–c}$$

where $\bar{u}_j$ are the values that the variable $\bar{U}$ and its derivatives changed of sign at the nodes of the finite element. As a consequence, $\psi_j = \psi_j(x,y)$ are the corresponding interpolating two-dimensional polynomials and they

belong to the family of the Hermite polynomials. It is important to note that they are the same shape polynomial usually used for a KPM element, that is, ψ_j with $j = 1, 2, 3, \ldots, r$, interpolates the values that the variables $\bar{U}, -\partial\bar{U}/\partial x, -\partial\bar{U}/\partial y$ (and eventually the second-order derivatives of $\bar{U}$ changed of sign if a higher number of nodes per FE is considered) assume at the FE nodes. The vector $\bar{\mathbf{u}}$ collects all the nodal values $\bar{u}_j$; these values must be related to the nodal values of the kinematic variables (deflection, rotations, and eventually the curvatures). If $\mathbf{u}$ is the vector that collects the nodal values of the kinematic variables, it can be related to $\bar{\mathbf{u}}$ by the following relationship:

$$\bar{\mathbf{u}} = \mathbf{B}\mathbf{u}; \quad \mathbf{B} = (\mathbf{I} + \mathbf{C})^{-1} \tag{26}$$

$\mathbf{I}$ being the identity matrix, while $\mathbf{C}$ is a constant square matrix whose evaluation is very simple, as shown in detail in the "Appendix A." However, here it is important to stress that matrix $\mathbf{C}$ depends only on the shape polynomials collected in the vector $\boldsymbol{\psi}$, besides the mechanical and material proprieties of the element.

Using Eq. (26) in Eq. (25a), the approximation of $\bar{U}$ can be rewritten as follows:

$$\bar{U} \approx \boldsymbol{\psi}^T \mathbf{B}\mathbf{u} \tag{27}$$

Then, by substituting Eq. (27) into Eqs. (25), the interdependent shape polynomials for the eigenfunction of the kinematic variables are obtained, these are $\boldsymbol{\psi}_w$, $\boldsymbol{\psi}_{\varphi_x}$ and $\boldsymbol{\psi}_{\varphi_y}$:

$$\begin{aligned}
U &\approx \boldsymbol{\psi}_w^T \mathbf{u}; \quad \boldsymbol{\psi}_U^T = \left(\boldsymbol{\psi}^T - \left(\frac{r_I}{r_A} + \frac{D}{S}\right)\nabla^2\boldsymbol{\psi}^T\right)\mathbf{B} \\
\Phi_x &\approx \boldsymbol{\psi}_{\Phi_x}^T \mathbf{u}; \quad \boldsymbol{\psi}_{\Phi_y}^T = \left(-\frac{\partial\boldsymbol{\psi}^T}{\partial x} + \frac{r_I}{r_A}\frac{\partial\nabla^2\boldsymbol{\psi}^T}{\partial x}\right)\mathbf{B} \\
\Phi_y &\approx \boldsymbol{\psi}_{\Phi_y}^T \mathbf{u}; \quad \boldsymbol{\psi}_{\Phi_y}^T = \left(-\frac{\partial\boldsymbol{\psi}^T}{\partial y} + \frac{r_I}{r_A}\frac{\partial\nabla^2\boldsymbol{\psi}^T}{\partial y}\right)\mathbf{B}
\end{aligned} \tag{28a–f}$$

It is worthy to note that these shape polynomials are related to the well-known shape polynomials $\boldsymbol{\psi}$, usually used to approximate the deflection of the KPM and listed in several books (i.e., see [5]). This means that the proposed shape polynomials for the MPM are very simple to obtain. Moreover, if the shear and rotary effects are neglected, that is, if $r_I = 0$ and $S \to \infty$, the terms in Eqs. (28) related to the Laplace operator become zero, and the matrix $\mathbf{B}$ coincides with the identity matrix (see the "Appendix B"). Thus, the shape polynomials proposed here degenerate in the well-known Hermite shape polynomials usually used for the KPM, which are

$$\boldsymbol{\psi}_w^T = \boldsymbol{\psi}^T; \quad \boldsymbol{\psi}_{\Phi_x}^T = -\frac{\partial\boldsymbol{\psi}^T}{\partial x}; \quad \boldsymbol{\psi}_{\Phi_y}^T = -\frac{\partial\boldsymbol{\psi}^T}{\partial y} \tag{29a–c}$$

This result implies that the KPM can be considered as a special case of the proposed approach. As it is showed in the "Appendix B," the new shape polynomials obviously do not depend on the density mass or by its mechanical proprieties, but on the ratio between the shear and bending stiffness (then by the Poisson's ratio and shear factor).

In some way, a similar result has been obtained by Reddy [26] for the static problem of the Timoshenko beam. He proposes a class of shape polynomials obtained by the exact solution of the homogenous governing equations. As a result, he obtains the exact interdependent shape polynomials. Unfortunately, his approach is limited only to a third-order polynomial approximation for the deflection. On the contrary, the present approach based on the use of the fictitious deflection enables one to consider any order of approximation for the kinematic variables, as shown in [15,16], for the static problem of the Timoshenko beam and MPM, and in the present work, for the dynamic analysis of the MPM.

It can be noted that the shape polynomials proposed here are obtained using the exact differential solution of the simplified version of the MPM. This means that these polynomials are interdependent, in the sense that they take into account the exact interdependences between the kinematic variables. As a matter of fact, substituting Eqs. (24) into Eq. (1), and using the approximated expression of the eigenfunction of the kinematic variables given into Eqs. (28), the following approximations for the shear angle strains are obtained:

$$\gamma_x \approx \frac{D}{S}\frac{\partial\nabla^2\boldsymbol{\psi}^T}{\partial x}\mathbf{B}\mathbf{u}e^{i\omega t}; \quad \gamma_y \approx \frac{D}{S}\frac{\partial\nabla^2\boldsymbol{\psi}^T}{\partial y}\mathbf{B}\mathbf{u}e^{i\omega t}; \tag{30a–b}$$

Then, expressing the shear angle strain by substituting $\bar{w} = \bar{U}e^{i\omega t}$ into Eqs. (18) and by dividing the result for S, and using Eqs. (27), the Eqs. (30) are exactly satisfied. This shows that the proposed shape polynomials take into account the differential link between the kinematic variables; this aspect cannot be satisfied if independent approximations are chosen for them, causing the well-known shear-locking phenomenon. Several authors demonstrated that for the MPM, the shear-locking phenomenon stems due to the inability of the model to reproduce the thin-plate condition [1,2,5,27], that is, $\gamma_x = \gamma_y = 0$. This approach overcomes this drawback because as the plate tends to the thin-plate condition, that is, when S tends to infinity, Eqs. (30) corresponds to neglecting values of the shear angle strains.

6 The element stiffness and mass matrices

In order to obtain the element stiffness and mass matrices, the interdependent shape polynomials for the kinematic variables derived in the previous section are used in the following weak formulation statement:

$$
\begin{aligned}
&D\int_{\Omega_e}\left[\frac{\partial v_2}{\partial x}\left(\frac{\partial \boldsymbol{\Phi}_x}{\partial x}+\nu\frac{\partial \boldsymbol{\Phi}_y}{\partial y}\right)+\frac{\partial v_3}{\partial y}\left(\frac{\partial \boldsymbol{\Phi}_y}{\partial y}+\nu\frac{\partial \boldsymbol{\Phi}_x}{\partial x}\right)+\frac{(1-\nu)}{2}\left(\frac{\partial v_2}{\partial y}+\frac{\partial v_3}{\partial x}\right)\left(\frac{\partial \boldsymbol{\Phi}_x}{\partial y}+\frac{\partial \boldsymbol{\Phi}_y}{\partial x}\right)\right]\mathrm{d}\boldsymbol{\Omega}\\
&+S\int_{\Omega_e}\left[\left(v_2+\frac{\partial v_1}{\partial x}\right)\left(\boldsymbol{\Phi}_x+\frac{\partial U}{\partial x}\right)+\left(v_3+\frac{\partial v_1}{\partial y}\right)\left(\boldsymbol{\Phi}_y+\frac{\partial U}{\partial y}\right)\right]\mathrm{d}\boldsymbol{\Omega}+\\
&-\omega^2\int_{\boldsymbol{\Omega}_e}\left[\boldsymbol{r}_A v_1 U-\boldsymbol{r}_I v_2\frac{\partial U}{\partial x}-r_I v_3\frac{\partial U}{\partial y}\right]\mathrm{d}\boldsymbol{\Omega}=\int_{\boldsymbol{\Gamma}_e} v_1 Q_n\mathrm{d}\boldsymbol{\Gamma}+\int_{\boldsymbol{\Gamma}_e} v_2 M_x^{(n)}\mathrm{d}\boldsymbol{\Gamma}+\int_{\boldsymbol{\Gamma}_e} v_3 M_y^{(n)}\mathrm{d}\boldsymbol{\Gamma}
\end{aligned}
\tag{31}
$$

v_1, v_2 and v_3 being three distinct weight functions. $\boldsymbol{\Omega}_e$ is the generic FE domain, $\boldsymbol{\Gamma}_e$ is its boundary closed line, Q_n is the shear force acting on the FE boundary characterized by the point normal vector $\mathbf{n}$; $M_x^{(n)}$ and $M_y^{(n)}$ are the components of the vector moment $\mathbf{M}^{(n)}$ acting on the same boundary. The first two integrals of this relationship provide the element stiffness matrix, while the third one provides the element mass matrix. Using the shape polynomials given in Eqs. (29), and setting $v_1 = \psi_{U,j}$, $v_2 = \psi_{\boldsymbol{\Phi}_x,j}$ and $v_3 = \psi_{\boldsymbol{\Phi}_y,j}$ with $j = 1, 2, \ldots, n$, with the aim of applying the Ritz–Galerkin FE approach, the following stiffness and mass matrices are obtained in compact form:

$$
\begin{aligned}
\mathbf{K} = {} & D\int_{\boldsymbol{\Omega}_e}\left[\frac{\partial \boldsymbol{\psi}_{\boldsymbol{\Phi}_x}}{\partial x}\left(\frac{\partial \boldsymbol{\psi}_{\boldsymbol{\Phi}_x}^T}{\partial x}+\boldsymbol{\nu}\frac{\partial \boldsymbol{\psi}_{\boldsymbol{\Phi}_y}^T}{\partial y}\right)+\frac{\partial \boldsymbol{\psi}_{\boldsymbol{\Phi}_y}}{\partial y}\left(\frac{\partial \boldsymbol{\psi}_{\boldsymbol{\Phi}_y}^T}{\partial y}+\boldsymbol{\nu}\frac{\partial \boldsymbol{\psi}_{\boldsymbol{\Phi}_x}^T}{\partial x}\right)\right]\mathrm{d}\boldsymbol{\Omega}\\
&+\int_{\boldsymbol{\Omega}_e}\frac{D\,(1-\nu)}{2}\left(\frac{\partial \boldsymbol{\psi}_{\boldsymbol{\Phi}_x}}{\partial y}+\frac{\partial \boldsymbol{\psi}_{\boldsymbol{\Phi}_y}}{\partial x}\right)\left(\frac{\partial \boldsymbol{\psi}_{\boldsymbol{\Phi}_x}^T}{\partial y}+\frac{\partial \boldsymbol{\psi}_{\boldsymbol{\Phi}_y}^T}{\partial x}\right)\mathrm{d}\boldsymbol{\Omega}\\
&+S\int_{\boldsymbol{\Omega}_e}\left[\left(\boldsymbol{\psi}_{\boldsymbol{\Phi}_x}+\frac{\partial \boldsymbol{\psi}_U}{\partial x}\right)\left(\boldsymbol{\psi}_{\boldsymbol{\Phi}_x}^T+\frac{\partial \boldsymbol{\psi}_U^T}{\partial x}\right)+\left(\boldsymbol{\psi}_{\boldsymbol{\Phi}_y}+\frac{\partial \boldsymbol{\psi}_U}{\partial y}\right)\left(\boldsymbol{\psi}_{\boldsymbol{\Phi}_y}^T+\frac{\partial \boldsymbol{\psi}_U^T}{\partial y}\right)\right]\mathrm{d}\boldsymbol{\Omega};\\
\mathbf{M} = {} & \int_{\boldsymbol{\Omega}_e}\left[r_A\boldsymbol{\psi}_U\boldsymbol{\psi}_U^T-r_I\boldsymbol{\psi}_{\boldsymbol{\Phi}_x}\frac{\partial \boldsymbol{\psi}_U^T}{\partial x}-r_I\boldsymbol{\psi}_{\boldsymbol{\Phi}_y}\frac{\partial \boldsymbol{\psi}_U^T}{\partial y}\right]\mathrm{d}\boldsymbol{\Omega}
\end{aligned}
\tag{32a–b}
$$

These formulations of the element stiffness and mass matrices will be used in the numerical example to investigate the free frequencies of square plates having different boundary conditions.

7 Numerical examples

In order to show the performance of the proposed FEM model, the five square plates represented in Fig. 1 are considered; they correspond to different combinations of boundary conditions, specifically simply supported (S), clamped (C), or free (F). The corresponding boundary equations are given by

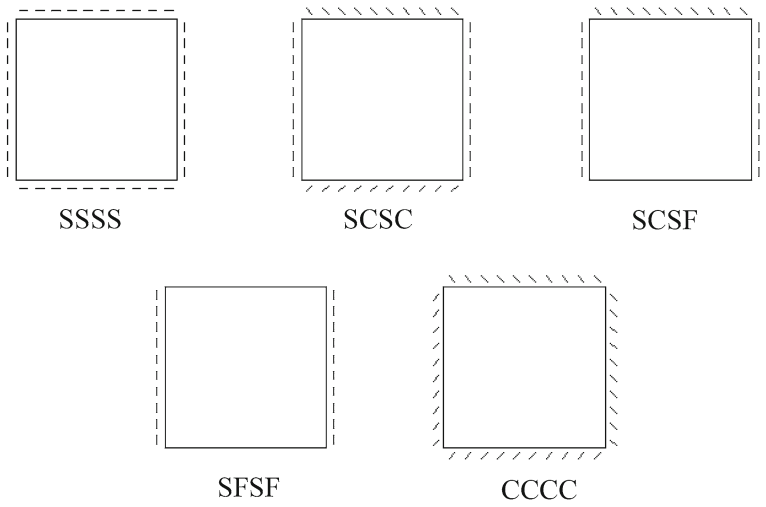

Fig. 1 Analysis cases

$$\begin{aligned} &\text{S: } w = 0; \quad \varphi_s = 0; \quad M_n = 0 \\ &\text{C: } w = 0; \quad \varphi_n = 0; \quad \varphi_s = 0 \\ &\text{F: } Q_n = 0; \quad M_n = 0; \quad M_{ns} = 0 \end{aligned} \tag{33a–c}$$

where the subscripts n and s represent the normal and tangent direction of the edge plate, respectively; φ_n and φ_s represent the generalized rotation around the directions s and n, respectively; Q_n, M_n, and M_{ns} are the shear force, the bending, and twisting moment acting on the edge of the plate.

In this work, the results are given in terms of the dimensionless frequencies β, defined as follows:

$$\beta = \omega L^2 \sqrt{\frac{\rho h}{D}} \tag{34}$$

L being the length of the square plate side.

The proposed FE model was applied within the four-nodes element with 3 degrees of freedom for each node, that is, assuming 12 degrees of freedom for each element. The plates are discretized in n_d^2 FEs, n_d being a mesh index giving the number of subdivisions of each plate side.

First, the SSSS plate that is all-round simply supported plate is considered. For this case, the frequencies corresponding to the "simplified" version of the Mindlin plate can be obtained in closed form by assuming for fictitious deflection $\overline{w}$ the following solution:

$$\bar{w} = \bar{U} \mathrm{e}^{i\omega t}; \quad \bar{U} = A \sin\left(\frac{n\pi}{L_x} x\right) \sin\left(\frac{m\pi}{L_y} y\right) \tag{35a,b}$$

where n and m are integer positive numbers and A is an arbitrary constant; L_x and L_y are the lengths of the plate sides; in the examples hereinafter, they are assumed equal each other: $L = L_x = L_y$. It is not difficult to verify that the above solution satisfies the boundary conditions in Eqs. (33a). Then, using Eqs. (35) in the governing equation given in Eq. (23), the following closed-form expression is obtained for the frequencies of the plate:

$$\omega^2 = \frac{\delta^2}{\frac{r_A}{D}\left[1 + \left(\frac{r_I}{r_A} + \frac{D}{S}\right)\delta\right]}; \quad \delta = \left(\frac{n\pi}{L_x}\right)^2 + \left(\frac{m\pi}{L_y}\right)^2 \tag{36a,b}$$

The same relationship was proposed in [24] considering again the simplified version of the MPM. In Table 1, the lowest nine dimensionless frequencies obtained for the plate SSSS with ratio $h/L = 0.01$ by the FEM are showed and compared with the exact dimensionless frequencies obtained by using Eqs. (34) and (36). The results show the good level of accuracy of the model, even for low value of the mesh index, as it can be better evidenced in Table 2, where the percentage errors are shown together with the total number of degrees of freedom (DOFs) related to mesh index n_d.

Table 1 First nine dimensionless frequencies $\beta = \omega L^2\sqrt{\rho h/D}$ of the SSSS plate with $h/L = 0.01$; $\nu = 0.3$; $\chi = 0.86667$

Eqs. (34)–(36)		19.73	49.30	49.30	78.85	98.52	98.52	128.01	128.01	167.28
	n_d	β_1	β_2	β_3	β_4	β_5	β_6	β_7	β_8	β_9
Proposed FEM model	2	18.02	50.91	50.91	108.53	124.37	207.74	207.74	–	–
	4	19.14	47.37	47.37	72.02	96.11	96.11	116.36	116.36	157.02
	6	19.45	48.27	48.31	75.02	96.73	96.73	120.40	120.51	161.83
	8	19.57	48.70	48.70	76.50	97.33	97.33	123.14	123.14	165.78
	10	19.63	48.91	48.91	77.28	97.70	97.70	124.68	124.68	166.10
	20	19.71	49.20	49.20	78.43	98.30	98.30	127.10	127.10	166.90
	30	19.72	49.26	49.26	78.66	98.42	98.42	127.60	127.60	167.11

Table 2 Percentage errors for the first nine frequencies of the SSSS plate with $h/L = 0.01$; $\nu = 0.3$; $\chi = 0.86667$

n_d	DOFs	β_1	β_2	β_3	β_4	β_5	β_6	β_7	β_8	β_9
2	7	8.69	3.25	3.25	37.65	26.23	110.86	62.28	–	–
4	39	2.98	3.92	3.92	8.66	2.45	2.45	9.10	9.10	6.14
6	95	1.41	2.10	2.02	4.86	1.82	1.82	5.95	5.86	3.26
8	175	0.81	1.23	1.23	2.97	1.21	1.21	3.81	3.81	0.89
10	279	0.52	0.81	0.81	1.98	0.83	0.83	2.60	2.60	0.70
20	1,159	0.13	0.21	0.21	0.52	0.23	0.23	0.71	0.71	0.23
30	2,639	0.06	0.09	0.09	0.24	0.10	0.10	0.32	0.32	0.10

Table 3 Comparison of the first nine dimensionless frequencies $\beta = \omega L^2\sqrt{\rho h/D}$ for the SSSS plate, with and without considering the higher-order time derivative contributions, assuming $\nu = 0.3$ and $\chi = 0.86667$

	β_1	β_2	β_3	β_4	β_5	β_6	β_7	β_8	β_9
$h/L = 0.01$									
Eqs. (34)–(36)	19.732	49.304	49.304	78.845	98.522	98.522	128.011	128.011	167.282
Hashemi and Arsajani [28]	19.732	49.305	49.305	78.846	98.522	98.522	128.011	128.011	167.282
Differences (%)	0.000	0.000	0.000	0.000	0.000	0.000	0.000	0.000	0.000
$h/L = 0.05$									
Eqs. (34)–(36)	19.567	48.293	48.293	76.306	94.605	94.605	121.516	121.516	156.446
Hashemi and Arsajani [28]	19.568	48.301	48.301	76.336	94.661	94.661	121.632	121.632	156.685
Differences (%)	0.003	0.016	0.016	0.039	0.059	0.059	0.095	0.095	0.153
$h/L = 0.1$									
Eqs. (36)–(36)	19.077	45.492	45.492	69.715	84.838	84.838	106.207	106.207	132.613
Hashemi and Arsajani [28]	19.084	45.585	45.585	70.022	85.365	85.365	107.178	107.178	134.359
Differences (%)	0.039	0.203	0.203	0.440	0.622	0.622	0.913	0.913	1.316
$h/L = 0.2$									
Eqs. (34)–(36)	17.429	37.773	37.773	54.090	63.529	63.529	76.167	76.167	90.953
Hashemi and Arsajani [28]	17.506	38.385	38.385	55.586	65.719	65.719	79.476	79.476	95.809
Differences (%)	0.441	1.619	1.619	2.766	3.448	3.448	4.344	4.344	5.339

It is worthy to note that, as the proposed FE model is based on the simplified version of the MPM equations, the above results are free of the higher-order time derivative effects. As discussed above, this contribution provides not very appreciable effects for the lowest frequencies of a thin plate (see Table 1). To evidence this aspect, the dimensionless frequencies of the SSSS plate are considered for the ratios $h/L = 0.01, 0.05, 0.1$, and 0.2, both including and neglecting the higher-order time derivative contribution. For the dimensionless frequencies including the higher-order derivative effects, one refers to [28], where the authors propose an analytical solution for the plate frequencies obtained by solving the exact characteristic equation.

In Table 3, the dimensionless frequencies obtained by Eqs. (34)–(36) and the analogous ones proposed in [28] are shown together with the corresponding percentage differences. The comparison shows that for the ratio $h/L = 0.01$, there is a practical coincidence of the present solution with one proposed in [28]. For $h/L = 0.05$, the percentage differences are very low, not exceeding the 0.15 %. Higher percentage differences can be observed for the case $h/L = 0.1$ (of about 1.3 % for the ninth frequency). More significant differences are observed for the plate of the ratio $h/L = 0.2$. However, the last two cases are representative of very thick

Table 4 First nine dimensionless frequencies $\beta = \omega L^2\sqrt{\rho h/D}$ of the SCSC plate with $h/L = 0.01$; $\nu = 0.3$; $\chi = 0.86667$

Hashemi and Arsajani [28]		28.93	54.67	69.19	94.37	102.01	128.69	139.78	154.22	169.81
	n_d	β_1	β_2	β_3	β_4	β_5	β_6	β_7	β_8	β_9
Proposed FEM model	2	25.81	50.91	87.48	117.83	207.74	–	–	–	–
	4	27.72	51.43	66.68	85.10	98.48	125.59	125.67	138.74	174.56
	6	28.34	52.89	67.75	88.89	99.28	126.76	129.67	144.81	167.40
	8	28.58	53.59	68.30	90.95	100.18	127.26	133.08	147.97	167.61
	10	28.70	53.96	68.60	92.07	100.74	127.66	135.15	149.88	168.11
	20	28.87	54.49	69.04	93.75	101.66	128.39	138.49	153.00	169.27
	30	28.90	54.59	69.13	94.09	101.85	128.55	139.20	153.66	169.56

Table 5 Percentage differences for the first nine frequencies of the SCSC plate with $h/L = 0.01$; $\nu = 0.3$; $\chi = 0.86667$: comparison with Hashemi and Arsajani [28]

n_d	DOFs	β_1	β_2	β_3	β_4	β_5	β_6	β_7	β_8	β_9
2	5	10.77	6.89	26.44	24.86	103.64	–	–	–	–
4	33	4.16	5.94	3.63	9.82	3.46	2.41	10.10	10.04	2.80
6	85	2.03	3.27	2.09	5.80	2.68	1.50	7.23	6.10	1.42
8	161	1.18	1.98	1.29	3.63	1.79	1.11	4.79	4.05	1.29
10	261	0.77	1.31	0.86	2.44	1.24	0.80	3.31	2.81	1.00
20	1121	0.20	0.34	0.22	0.65	0.35	0.23	0.92	0.79	0.32
30	2581	0.09	0.15	0.09	0.29	0.16	0.11	0.42	0.36	0.15

Table 6 First nine dimensionless frequencies $\beta = \omega L^2\sqrt{\rho h/D}$ of the SCSF plate with $h/L = 0.01$; $\nu = 0.3$; $\chi = 0.86667$

Hashemi and Arsajani [28]		12.67	32.99	41.65	62.86	72.22	90.42	102.79	111.57	131.00
	n_d	β_1	β_2	β_3	β_4	β_5	β_6	β_7	β_8	β_9
Proposed FEM model	2	12.54	30.39	45.44	60.78	82.63	112.65	128.18	202.31	218.68
	4	12.64	32.01	41.86	59.65	69.83	91.87	94.73	106.40	127.03
	6	12.67	32.53	41.81	61.18	70.90	91.23	97.95	108.40	129.09
	8	12.67	32.74	41.74	61.86	71.43	90.88	99.78	109.54	129.66
	10	12.68	32.84	41.72	62.23	71.71	90.75	100.81	110.23	130.06
	20	12.68	32.99	41.68	62.75	72.13	90.54	102.36	111.27	130.77
	30	12.68	33.01	41.67	62.84	72.20	90.49	102.66	111.47	130.92

Table 7 Percentage differences for the first nine frequencies of the SCSF plate with $h/L = 0.01$; $\nu = 0.3$; $\chi = 0.86667$: comparison with Hashemi and Arsajani [28]

n_d	DOFs	β_1	β_2	β_3	β_4	β_5	β_6	β_7	β_8	β_9
2	10	1.06	7.90	9.11	3.31	14.42	24.59	24.70	81.34	66.93
4	44	0.22	2.99	0.51	5.10	3.30	1.60	7.84	4.63	3.03
6	102	0.03	1.40	0.39	2.67	1.82	0.90	4.71	2.84	1.45
8	184	0.01	0.77	0.23	1.59	1.09	0.51	2.93	1.82	1.02
10	290	0.04	0.45	0.18	1.01	0.70	0.37	1.93	1.20	0.72
20	1,180	0.07	0.02	0.09	0.18	0.12	0.14	0.42	0.27	0.17
30	2,670	0.07	0.05	0.06	0.03	0.02	0.08	0.12	0.09	0.06

plate. Nevertheless, as expected, for thin plate, the frequencies obtained by considering the higher-order time derivative contributions are practically coincident with the analogous ones obtained neglecting them.

Results proposed in [28] for the SCSC, SFSF, and SCSF plates with ratio $h/L = 0.01$ were also considered. Comparison shows a good accuracy of the proposed FE model. In Table 4, the comparison is made for the SCSC plate with $h/L = 0.01$, whereas in Table 5 the corresponding percentage differences are showed evidencing the good performance of the proposed FE model even with respect to the number of DOFs corresponding to each choice of the mesh index n_d. In Tables 6, 7, 8, and 9, results are listen for the SCSF and SFSF plate when h/L is fixed at 0.01.

In all the tables, the results are obtained for the mesh indices $n_d = 2, 4, 6, 8, 10$ to evidence the performance of the method. The mesh indices $n_d = 20, 30$ are considered to show as the method converges to the exact results.

Table 8 First nine dimensionless frequencies $\beta = \omega L^2\sqrt{\rho h/D}$ of the SFSF plate with $h/L = 0.01$; $\nu = 0.3$; $\chi = 0.86667$

Hashemi and Arsajani [28]		9.63	16.10	36.61	38.90	46.64	70.48	75.06	87.82	95.78
	n_d	β_1	β_2	β_3	β_4	β_5	β_6	β_7	β_8	β_9
Proposed FEM model	2	9.89	16.11	33.92	43.81	50.91	67.88	80.10	109.10	118.23
	4	9.71	16.13	35.77	39.57	46.68	67.68	72.75	90.18	96.06
	6	9.67	16.13	36.22	39.24	46.74	68.93	73.80	88.97	96.22
	8	9.65	16.13	36.43	39.11	46.75	69.66	74.36	88.54	96.21
	10	9.64	16.13	36.52	39.05	46.74	70.00	74.64	88.31	96.13
	20	9.63	16.13	36.65	38.95	46.71	70.47	75.03	87.97	95.95
	30	9.63	16.13	36.67	38.93	46.70	70.55	75.10	87.90	95.90

Table 9 Percentage differences for the first nine frequencies of the SFSF plate with $h/L = 0.01$; $\nu = 0.3$; $\chi = 0.86667$: comparison with Hashemi and Arsajani [28]

n_d	DOFs	β_1	β_2	β_3	β_4	β_5	β_6	β_7	β_8	β_9
2	15	2.69	0.08	7.35	12.61	9.15	3.70	6.72	24.24	23.44
4	55	0.88	0.20	2.30	1.70	0.08	3.97	3.08	2.69	0.29
6	119	0.42	0.20	1.07	0.87	0.21	2.20	1.67	1.32	0.46
8	207	0.25	0.21	0.50	0.54	0.24	1.17	0.92	0.82	0.45
10	319	0.17	0.21	0.24	0.37	0.21	0.69	0.56	0.56	0.37
20	1,239	0.06	0.20	0.11	0.12	0.15	0.02	0.03	0.18	0.18
30	2,759	0.04	0.18	0.16	0.07	0.12	0.10	0.06	0.10	0.13

Table 10 First six dimensionless frequencies $\beta = \omega L^2\sqrt{\rho h/D}$ of the CCCC plate with $h/L = 0.005$; $\nu = 0.3$; $\chi = 5/6$

Robert [29]		35.99	73.41	73.41	108.31	131.61	132.20
	n_d	β_1	β_2	β_3	β_4	β_5	β_6
Proposed FEM model	2	35.10	87.52	87.52	–	–	–
	4	34.30	70.01	70.01	98.01	127.50	129.54
	6	35.09	71.22	71.22	101.20	128.49	129.61
	8	35.44	72.00	72.00	103.64	129.31	130.18
	10	35.62	72.44	72.44	105.06	129.92	130.70
	20	35.88	73.11	73.11	107.30	131.02	131.68
	30	35.93	73.24	73.25	107.76	131.26	131.91

Table 11 Percentage differences for the first six frequencies of the CCCC plate with $h/L = 0.005$; $\nu = 0.3$; $\chi = 5/6$: comparison with Robert [29]

n_d	DOFs	β_1	β_2	β_3	β_4	β_5	β_6
2	3	2.46	19.21	19.21	–	–	–
4	27	4.69	4.64	4.64	9.50	3.12	2.02
6	75	2.51	2.98	2.98	6.56	2.36	1.96
8	147	1.51	1.92	1.92	4.31	1.74	1.53
10	243	1.01	1.32	1.32	2.99	1.28	1.14
20	1,083	0.29	0.41	0.41	0.93	0.44	0.39
30	2,523	0.15	0.23	0.22	0.51	0.26	0.23

In Table 10, the first six dimensionless frequencies of the CCCC plate with $h/L = 0.005$ are listed. Comparison is made with the analogous results reported in [29]. In this example too, a very good approximation is provided by the proposed model, as it is better evidenced in Table 11 where the corresponding percentage differences are reported.

Lastly, in Table 12 and 13, the first nine dimensionless frequencies of the SSSS plate with $h/L = 0.2$ and the corresponding percentage error are given, making the comparison with the exact frequencies obtained by Eqs. (36) and (38).

8 Conclusions

In this paper, a free-locking FE model is proposed for the dynamic analysis of the Mindlin plate considering both shear deformation and rotary inertia effects. The work uses the simplified version of the Mindlin plate equations.

Table 12 First nine dimensionless frequencies $\beta = \omega L^2\sqrt{\rho h/D}$ of the SSSS plate with $h/L = 0.2$; $\nu = 0.3$; $\chi = 0.86667$ comparison with Eqs. (36)–(38)

Eqs. (36)–(38)		17.4287	37.773	37.773	54.0896	63.5289	63.5289	76.1668	76.1668	90.9526
	n_d	β_1	β_2	β_3	β_4	β_5	β_6	β_7	β_8	β_9
Proposed FEM model	2	16.46	48.39	48.39	98.67	109.53	209.81	209.81	0.00	0.00
	4	17.08	37.82	37.84	53.61	68.10	68.13	78.86	79.91	100.11
	6	17.26	37.67	37.77	53.61	65.53	65.53	77.19	77.26	96.20
	8	17.33	37.67	37.79	53.75	64.61	64.61	76.58	76.68	95.13
	10	17.37	37.74	37.74	53.84	64.20	64.20	76.36	76.36	93.70
	20	17.41	37.76	37.76	54.02	63.69	63.69	76.20	76.20	91.63
	30	17.42	37.77	37.77	54.06	63.60	63.60	76.18	76.18	91.25

Table 13 Percentage error for the first nine frequencies of the SSSS plate with $h/L = 0.2$; $\nu = 0.3$; $\chi = 0.86667$

n_d	DOFs	β_1	β_2	β_3	β_4	β_5	β_6	β_7	β_8	β_9
2	7	5.56	28.11	28.11	82.41	72.41	230.26	175.46	100.00	100.00
4	39	1.99	0.12	0.18	0.89	7.20	7.24	3.53	4.91	10.07
6	95	0.96	0.26	0.00	0.89	3.14	3.16	1.34	1.44	5.77
8	175	0.55	0.28	0.04	0.62	1.70	1.71	0.54	0.67	4.59
10	279	0.36	0.10	0.10	0.47	1.06	1.06	0.26	0.26	3.02
20	1,159	0.09	0.03	0.03	0.13	0.26	0.26	0.05	0.05	0.74
30	2,639	0.04	0.01	0.01	0.06	0.11	0.11	0.02	0.02	0.33

Specifically, the contribution of the higher-order time derivative is neglected, providing more consistent results than original Mindlin equations. Using these equations and introducing a new generalized variable (the fictitious deflection), a new class of interdependent Hermite shape polynomials has been derived. These polynomials have the remarkable property of taking into account the exact interdependence between the kinematic variables. The numerical results show that the proposed FE model provides very accurate results even for low-order FEs.

Finally, it is worthy to note that the Hermite shape polynomials have been related to the well-known Hermite shape polynomials used for the KPM FE. Remarkably, the latter turns out to be a special case of the proposed FE model.

Appendix A

A n-nodes finite element is taken into account and it is supposed that the vector $\bar{\mathbf{u}}$ to collects the nodal values of $\bar{U}$, of $-\partial\bar{U}/\partial x$, and of $-\partial\bar{U}/\partial y$. Likewise, the vector $\mathbf{u}$ collects the nodal values of U, Φ_x and Φ_y. If the jth, the $j+1$th and the $j+2$th element of $\bar{\mathbf{u}}$, ($\bar{u}_j$, $\bar{u}_{j+1}$ and $\bar{u}_{j+2}$), are the nodal values of $\bar{U}$, $-\partial\bar{U}/\partial x$ and $-\partial\bar{U}/\partial y$ at the node of coordinates $\left(x_j, y_j\right)$, using the relationships given in Eqs. (23) and the approximation for $\bar{U}$ given in Eq. (25a), the following expressions are obtained:

$$u_j = \bar{u}_j + \left[-\left(\frac{r_I}{r_A} + \frac{D}{S}\right) \nabla^2\boldsymbol{\psi}^T \Big|_{\substack{x=x_j \\ y=y_j}} \right] \bar{\mathbf{u}};$$

$$u_{j+1} = \bar{u}_{j+1} + \left[\frac{r_I}{r_A} \frac{\partial\nabla^2\boldsymbol{\psi}^T}{\partial x} \Big|_{\substack{x=x_j \\ y=y_j}} \right] \bar{\mathbf{u}};$$

$$u_{j+2} = \bar{u}_{j+2} + \left[\frac{r_I}{r_A} \frac{\partial\nabla^2\boldsymbol{\psi}^T}{\partial y} \Big|_{\substack{x=x_j \\ y=y_j}} \right] \bar{\mathbf{u}} \qquad \text{(A1a–c)}$$

where u_j, u_{j+1} and u_{j+2} are the nodal values of U, Φ_x and Φ_y at the node of coordinates $\left(x_j, y_j\right)$. Applying the above equations for all the n nodes of the element, that is, for $j = 1, 2, \ldots, n$, it is possible to write the following compact equation:

$$\mathbf{u} = (\mathbf{I} + \mathbf{C})\,\bar{\mathbf{u}} \tag{A1a–c}$$

where $\mathbf{C}$ is a constant square matrix of order $3n$ whose kth row is equal to:

(a) the function vector $-(r_I/r_A + D/S)\,\nabla^2\boldsymbol{\psi}^T$ evaluated at the corresponding nodal coordinates, if the u_k element is a deflection;
(b) the function vector $-r_I/r_A\,\partial\nabla^2\boldsymbol{\psi}^T/\partial x$ evaluated at the corresponding nodal coordinates, if the u_k element is a rotation Φ_x;
(c) the function vector $-r_I/r_A\,\partial\nabla^2\boldsymbol{\psi}^T/\partial y$ evaluated at the corresponding nodal coordinates, if the u_k element is a rotation Φ_y

Equation (26) in the text follows immediately from Eq. (A2)

If the vector $\bar{\mathbf{u}}$ collects also the nodal values of $-\partial^2\bar{U}/\partial x\,\partial y$, then the vector $\mathbf{u}$ collects also the nodal values of the twisting curvature $0.5\left(\partial\boldsymbol{\Phi}_y/\partial x + \partial\boldsymbol{\Phi}_x/\partial y\right)$. Then, the elements of Eq. (A2) must take into account that if the $j+3$th element of $\bar{\mathbf{u}}$, $(\bar{u}_{j+3})$, is the nodal values of $-\partial^2\bar{U}/\partial x\,\partial y$ at the node of coordinates $\left(x_j, y_j\right)$, using Eqs. (26a–b) one must writes

$$u_{j+3} = \bar{u}_{j+3} + \frac{r_I}{r_A}\left.\frac{\partial^2\nabla^2\boldsymbol{\psi}^T}{\partial x\,\partial y}\right|_{\substack{x = x_j \\ y = y_j}} \tag{A3}$$

Then, applying Eqs. (A1) and (A3) for all the n nodes of the element, that is, for $j = 1, 2, \ldots, n$, it is possible to obtain again the compact equation given in Eq. (A2), where $\mathbf{C}$ is a constant square matrix of order $4n$ whose kth row is equal to

(a) the function vector $-(r_I/r_A + D/S)\,\nabla^2\boldsymbol{\psi}^T$ evaluated at the corresponding nodal coordinates, if the u_k element is a deflection;
(b) the function vector $-r_I/r_A\,\partial\nabla^2\boldsymbol{\psi}^T/\partial x$ evaluated at the corresponding nodal coordinates, if the u_k element is a rotation Φ_x;
(c) the function vector $-r_I/r_A\,\partial\nabla^2\boldsymbol{\psi}^T/\partial y$ evaluated at the corresponding nodal coordinates, if the u_k element is a rotation Φ_y
(d) the function vector $-r_I/r_A\,\partial^2\nabla^2\boldsymbol{\psi}^T/\partial x\,\partial y$ evaluated at the corresponding nodal coordinates, if the u_k element is a twisting curvature $0.5\left(\partial\Phi_y/\partial x + \partial\Phi_x/\partial y\right)$.

In a similar way, other different choices of interpolated variables at the FE nodes can be made; however, the cases above represent the most used ones.

Appendix B

Let us consider a rectangular four-node FE as indicated in Fig. 2, having thickness h.

The related interdependent shape polynomials have the following expressions:

$$\boldsymbol{\psi}_U^T = \begin{pmatrix}
\frac{-6h^2\beta^2(1+\eta)\xi(\Gamma+\Omega)+\alpha^2(-1+\xi)(\beta^2(1+\eta)(-2+(-1+\eta)\eta+\xi+\xi^2)-6h^2\eta(\Gamma+\Omega))}{8\alpha^2\beta^2} \\
-\frac{(1+\eta)(\alpha^2(-1+\xi)^2(1+\xi)-2h^2(-1+3\xi)(\Gamma+\Omega))}{8\alpha} \\
\frac{(-1+\xi)(\beta^2(-1+\eta)(1+\eta)^2-2h^2(1+3\eta)(\Gamma+\Omega))}{8\beta} \\
\frac{6h^2\beta^2(-1+\eta)\xi(\Gamma+\Omega)-\alpha^2(-1+\xi)(\beta^2(-1+\eta)(-2+\eta+\eta^2+\xi+\xi^2)-6h^2\eta(\Gamma+\Omega))}{8\alpha^2\beta^2} \\
\frac{(-1+\eta)(\alpha^2(-1+\xi)^2(1+\xi)-2h^2(-1+3\xi)(\Gamma+\Omega))}{8\alpha} \\
\frac{(-1+\xi)(\beta^2(-1+\eta)^2(1+\eta)-2h^2(-1+3\eta)(\Gamma+\Omega))}{8\beta} \\
\frac{-6h^2\beta^2(-1+\eta)\xi(\Gamma+\Omega)+\alpha^2(1+\xi)(\beta^2(-1+\eta)(\eta+\eta^2+(-2+\xi)(1+\xi))-6h^2\eta(\Gamma+\Omega))}{8\alpha^2\beta^2} \\
\frac{(-1+\eta)(\alpha^2(-1+\xi)(1+\xi)^2-2h^2(1+3\xi)(\Gamma+\Omega))}{8\alpha} \\
-\frac{(1+\xi)(\beta^2(-1+\eta)^2(1+\eta)-2h^2(-1+3\eta)(\Gamma+\Omega))}{8\beta} \\
\frac{6h^2\beta^2(1+\eta)\xi(\Gamma+\Omega)-\alpha^2(1+\xi)(\beta^2(1+\eta)((-1+\eta)\eta+(-2+\xi)(1+\xi))-6h^2\eta(\Gamma+\Omega))}{8\alpha^2\beta^2} \\
-\frac{(1+\eta)(\alpha^2(-1+\xi)(1+\xi)^2-2h^2(1+3\xi)(\Gamma+\Omega))}{8\alpha} \\
-\frac{(1+\xi)(\beta^2(-1+\eta)(1+\eta)^2-2h^2(1+3\eta)(\Gamma+\Omega))}{8\beta}
\end{pmatrix} [\mathbf{I} + \mathbf{C}]^{-1} \tag{B1}$$

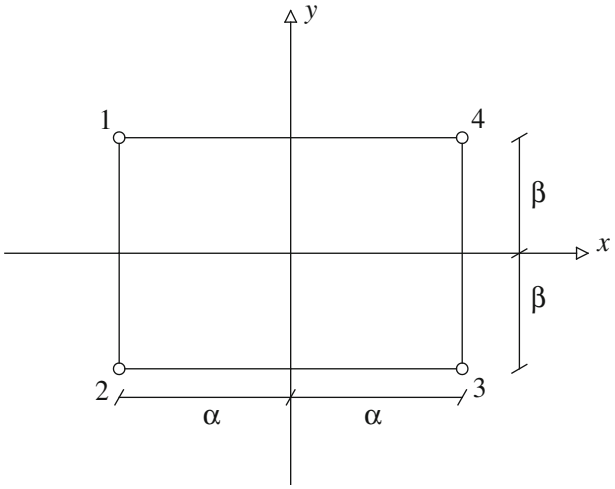

Fig. 2 Rectangular four-nodes element

$$\boldsymbol{\psi}_{\boldsymbol{\Phi}_x}^T = \begin{pmatrix} \frac{6h^2\beta^2\Gamma(1+\eta)+\alpha^2(6h^2\Gamma\eta-\beta^2(1+\eta)(-3-\eta+\eta^2+3\xi^2))}{8\alpha^3\beta^2} \\ \frac{(1+\eta)(-6h^2\Gamma+\alpha^2(-1+\xi)(1+3\xi))}{8\alpha^2} \\ \frac{-\beta^2(-1+\eta)(1+\eta)^2+2h^2\Gamma(1+3\eta)}{8\alpha\beta} \\ \frac{-6h^2\beta^2\Gamma(-1+\eta)+\alpha^2(-6h^2\Gamma\eta+\beta^2(-1+\eta)(-3+\eta+\eta^2+3\xi^2))}{8\alpha^3\beta^2} \\ \frac{(-1+\eta)(6h^2\Gamma+\alpha^2(1+(2-3\xi)\xi))}{8\alpha^2} \\ \frac{-\beta^2(-1+\eta)^2(1+\eta)+2h^2\Gamma(-1+3\eta)}{8\alpha\beta} \\ \frac{6h^2\beta^2\Gamma(-1+\eta)+\alpha^2(6h^2\Gamma\eta-\beta^2(-1+\eta)(-3+\eta+\eta^2+3\xi^2))}{8\alpha^3\beta^2} \\ -\frac{(-1+\eta)(-6h^2\Gamma+\alpha^2(1+\xi)(-1+3\xi))}{8\alpha^2} \\ \frac{2h^2\Gamma(1-3\eta)+\beta^2(-1+\eta)^2(1+\eta)}{8\alpha\beta} \\ \frac{-6h^2\beta^2\Gamma(1+\eta)+\alpha^2(-6h^2\Gamma\eta+\beta^2(1+\eta)(-3-\eta+\eta^2+3\xi^2))}{8\alpha^3\beta^2} \\ \frac{(1+\eta)(-6h^2\Gamma+\alpha^2(1+\xi)(-1+3\xi))}{8\alpha^2} \\ \frac{\beta^2(-1+\eta)(1+\eta)^2-2h^2\Gamma(1+3\eta)}{8\alpha\beta} \end{pmatrix} [\mathbf{I}+\mathbf{C}]^{-1} \tag{B2}$$

$$\boldsymbol{\psi}_{\boldsymbol{\Phi}_y}^T = \begin{pmatrix} \frac{6h^2\beta^2\Gamma\xi-\alpha^2(-1+\xi)(-6h^2\Gamma+\beta^2(-3+3\eta^2+\xi+\xi^2))}{8\alpha^2\beta^3} \\ \frac{2h^2\Gamma(1-3\xi)+\alpha^2(-1+\xi)^2(1+\xi)}{8\alpha\beta} \\ -\frac{(-6h^2\Gamma+\beta^2(1+\eta)(-1+3\eta))(-1+\xi)}{8\beta^2} \\ \frac{-6h^2\beta^2\Gamma\xi+\alpha^2(-1+\xi)(-6h^2\Gamma+\beta^2(-3+3\eta^2+\xi+\xi^2))}{8\alpha^2\beta^3} \\ \frac{-\alpha^2(-1+\xi)^2(1+\xi)+2h^2\Gamma(-1+3\xi)}{8\alpha\beta} \\ \frac{(6h^2\Gamma+\beta^2(1+(2-3\eta)\eta))(-1+\xi)}{8\beta^2} \\ \frac{6h^2\beta^2\Gamma\xi-\alpha^2(1+\xi)(-6h^2\Gamma+\beta^2(-3+3\eta^2+(-1+\xi)\xi))}{8\alpha^2\beta^3} \\ \frac{-\alpha^2(-1+\xi)(1+\xi)^2+2h^2\Gamma(1+3\xi)}{8\alpha\beta} \\ \frac{(-6h^2\Gamma+\beta^2(-1+\eta)(1+3\eta))(1+\xi)}{8\beta^2} \\ \frac{-6h^2\beta^2\Gamma\xi+\alpha^2(1+\xi)(-6h^2\Gamma+\beta^2(-3+3\eta^2+(-1+\xi)\xi))}{8\alpha^2\beta^3} \\ \frac{\alpha^2(-1+\xi)(1+\xi)^2-2h^2\Gamma(1+3\xi)}{8\alpha\beta} \\ \frac{(-6h^2\Gamma+\beta^2(1+\eta)(-1+3\eta))(1+\xi)}{8\beta^2} \end{pmatrix} [\mathbf{I}+\mathbf{C}]^{-1} \tag{B3}$$

being:

$$\xi = \frac{x}{\alpha};\ \eta = \frac{y}{\beta};\quad \Omega = \frac{D}{Sh^2} = \frac{1-\nu}{6\chi};$$
$$\Gamma = \frac{r_I}{r_A h^2} = \frac{1}{12};\quad \mathbf{C} = 6\alpha\beta\left[\Gamma\mathbf{C}_1 + \Omega\mathbf{C}_2\right] \tag{B4a–c}$$

$$\mathbf{C}_1 = \begin{pmatrix}
\frac{\alpha^2+\beta^2}{4\alpha\beta} & \frac{-h}{3\beta} & \frac{h}{3\alpha} & -\frac{\beta}{4\alpha} & 0 & \frac{h}{6\alpha} & 0 & 0 & 0 & -\frac{\alpha}{4\beta} & -\frac{h}{6\beta} & 0 \\
\frac{2\alpha^2+\beta^2}{8h\beta} & -\frac{\alpha}{4\beta} & \frac{1}{6} & -\frac{\beta}{8h} & 0 & \frac{1}{12} & \frac{\beta}{8h} & 0 & -\frac{1}{12} & -\frac{2\alpha^2+\beta^2}{8h\beta} & -\frac{\alpha}{4\beta} & -\frac{1}{6} \\
-\frac{\alpha^2+2\beta^2}{8h\alpha} & \frac{1}{6} & -\frac{\beta}{4\alpha} & \frac{\alpha^2+2\beta^2}{8h\alpha} & -\frac{1}{6} & -\frac{\beta}{4\alpha} & -\frac{\alpha}{8h} & -\frac{1}{12} & 0 & \frac{\alpha}{8h} & \frac{1}{12} & 0 \\
-\frac{\beta}{4\alpha} & 0 & -\frac{h}{6\alpha} & \frac{\alpha^2+\beta^2}{4\alpha\beta} & -\frac{h}{3\beta} & -\frac{h}{3\alpha} & -\frac{\alpha}{4\beta} & -\frac{h}{6\beta} & 0 & 0 & 0 & 0 \\
-\frac{\beta}{8h} & 0 & -\frac{1}{12} & \frac{2\alpha^2+\beta^2}{8h\beta} & -\frac{\alpha}{4\beta} & -\frac{1}{6} & -\frac{2\alpha^2+\beta^2}{8h\beta} & -\frac{\alpha}{4\beta} & \frac{1}{6} & \frac{\beta}{8h} & 0 & \frac{1}{12} \\
-\frac{\alpha^2+2\beta^2}{8h\alpha} & \frac{1}{6} & -\frac{\beta}{4\alpha} & \frac{\alpha^2+2\beta^2}{8h\alpha} & -\frac{1}{6} & -\frac{\beta}{4\alpha} & -\frac{\alpha}{8h} & -\frac{1}{12} & 0 & \frac{\alpha}{8h} & \frac{1}{12} & 0 \\
0 & 0 & 0 & -\frac{\alpha}{4\beta} & \frac{h}{6\beta} & 0 & \frac{\alpha^2+\beta^2}{4\alpha\beta} & \frac{h}{3\beta} & -\frac{h}{3\alpha} & -\frac{\beta}{4\alpha} & 0 & -\frac{h}{6\alpha} \\
-\frac{\beta}{8h} & 0 & -\frac{1}{12} & \frac{2\alpha^2+\beta^2}{8h\beta} & -\frac{\alpha}{4\beta} & -\frac{1}{6} & -\frac{2\alpha^2+\beta^2}{8h\beta} & -\frac{\alpha}{4\beta} & \frac{1}{6} & \frac{\beta}{8h} & 0 & \frac{1}{12} \\
\frac{\alpha}{8h} & -\frac{1}{12} & 0 & -\frac{\alpha}{8h} & \frac{1}{12} & 0 & \frac{\alpha^2+2\beta^2}{8h\alpha} & \frac{1}{6} & -\frac{\beta}{4\alpha} & -\frac{\alpha^2+2\beta^2}{8h\alpha} & -\frac{1}{6} & -\frac{\beta}{4\alpha} \\
-\frac{\alpha}{4\beta} & \frac{h}{6\beta} & 0 & 0 & 0 & 0 & -\frac{\beta}{4\alpha} & 0 & \frac{h}{6\alpha} & \frac{\alpha^2+\beta^2}{4\alpha\beta} & \frac{h}{3\beta} & \frac{h}{3\alpha} \\
\frac{2\alpha^2+\beta^2}{8h\beta} & -\frac{\alpha}{4\beta} & \frac{1}{6} & -\frac{\beta}{8h} & 0 & \frac{1}{12} & \frac{\beta}{8h} & 0 & -\frac{1}{12} & -\frac{2\alpha^2+\beta^2}{8h\beta} & -\frac{\alpha}{4\beta} & -\frac{1}{6} \\
\frac{\alpha}{8h} & -\frac{1}{12} & 0 & -\frac{\alpha}{8h} & \frac{1}{12} & 0 & \frac{\alpha^2+2\beta^2}{8h\alpha} & \frac{1}{6} & -\frac{\beta}{4\alpha} & -\frac{\alpha^2+2\beta^2}{8h\alpha} & -\frac{1}{6} & -\frac{\beta}{4\alpha}
\end{pmatrix} \tag{B5}$$

$$\mathbf{C}_2 = \begin{pmatrix}
\frac{\alpha^2+\beta^2}{4\alpha\beta} & -\frac{h}{3\beta} & \frac{h}{3\alpha} & -\frac{\beta}{4\alpha} & 0 & \frac{h}{6\alpha} & 0 & 0 & 0 & -\frac{\alpha}{4\beta} & -\frac{h}{6\beta} & 0 \\
0 & 0 & 0 & 0 & 0 & 0 & 0 & 0 & 0 & 0 & 0 & 0 \\
0 & 0 & 0 & 0 & 0 & 0 & 0 & 0 & 0 & 0 & 0 & 0 \\
-\frac{\beta}{4\alpha} & 0 & -\frac{h}{6\alpha} & \frac{\alpha^2+\beta^2}{4\alpha\beta} & -\frac{h}{3\beta} & -\frac{h}{3\alpha} & -\frac{\alpha}{4\beta} & -\frac{h}{6\beta} & 0 & 0 & 0 & 0 \\
0 & 0 & 0 & 0 & 0 & 0 & 0 & 0 & 0 & 0 & 0 & 0 \\
0 & 0 & 0 & 0 & 0 & 0 & 0 & 0 & 0 & 0 & 0 & 0 \\
0 & 0 & 0 & -\frac{\alpha}{4\beta} & \frac{h}{6\beta} & 0 & \frac{\alpha^2+\beta^2}{4\alpha\beta} & \frac{h}{3\beta} & -\frac{h}{3\alpha} & -\frac{\beta}{4\alpha} & 0 & -\frac{h}{6\alpha} \\
0 & 0 & 0 & 0 & 0 & 0 & 0 & 0 & 0 & 0 & 0 & 0 \\
0 & 0 & 0 & 0 & 0 & 0 & 0 & 0 & 0 & 0 & 0 & 0 \\
-\frac{\alpha}{4\beta} & \frac{h}{6\beta} & 0 & 0 & 0 & 0 & -\frac{\beta}{4\alpha} & 0 & \frac{h}{6\alpha} & \frac{\alpha^2+\beta^2}{4\alpha\beta} & \frac{h}{3\beta} & \frac{h}{3\alpha} \\
0 & 0 & 0 & 0 & 0 & 0 & 0 & 0 & 0 & 0 & 0 & 0 \\
0 & 0 & 0 & 0 & 0 & 0 & 0 & 0 & 0 & 0 & 0 & 0
\end{pmatrix} \tag{B6}$$

References

1. Reddy, J.N.: A penalty plate bending element for the analysis of laminated anisotropic composite plates. Int. J. Numer. Methods Eng. **15**, 1187–1206 (1980)
2. Averill, R.C., Reddy, J.N.: On the behavior of plate elements based on the first-order shear deformation theory. Eng. Comput. **7**, 57–74 (1990)
3. Zienkiewicz, O.C., Taylor, R.L., To, J.M.: Reduced integration technique in general analysis of plates and shells. Int. J. Numer. Methods Eng. **3**, 275–290 (1971)
4. Hughes, T.J.R., Taylor, R.L., Kanoknukulchai, W.: Simple and efficient element for plate bending. Int. J. Numer. Methods Eng. **11**, 1529–1543 (1977)
5. Reddy, J.N.: An Introduction to the Finite Element Method, 2nd edn. McGraw-Hill, New York (1993)
6. Lee, S.W., Wong, C.: Mixed formulation finite elements for Mindlin theory plate bending. Int. J. Numer. Methods Eng. **18**, 1297–1311 (1982)
7. Auricchio, F., Taylor, R.L.: A triangular thick plate finite element with an exact thin limit. Finite Elem. Anal. Des. **19**, 57–68 (1995)
8. Lovadina, C.: Analysis of a mixed finite element method for the Reissner–Mindlin plate problems. Comput. Methods Appl. Mech. Eng. **163**, 71–85 (1998)

9. Hughes, T.J.R., Tezduyar, T.: Finite elements based upon Mindlin plate theory with particular reference to the four-node isoparametric element. J. Appl. Mech. **48**, 587–596 (1981)
10. Bathe, K.J.: Finite Element Procedures. Prentice-Hall/MIT, Englewood Cliffs (1996)
11. Zienkiewicz, O.C., Taylor, R.L.: The Finite Element Method, 5th edn. Butterworth-Heinemann, Oxford (2000)
12. Bletzinger, K., Bischoff, M., Ramm, E.: A unified approach for shear-locking-free triangular and rectangular shell finite elements. Comput. Struct. **75**, 321–334 (2000)
13. Nguyen-Xuan, H., Liu, G.R., Thai-Hoang, C., Nguyen-Thoi, T.: An edge-based smoothed finite element method (ES-FEM) with stabilized discrete shear gap technique for analysis of Reissner–Mindlin plates. Comput. Methods Appl. Mech. Eng. **199**, 471–489 (2010)
14. Liu, G.R., Nguyen-Thoi, T., Lam, Y.K.: An edge-based smoothed finite element method (ES-FEM) for static, free and forced vibration analyses of solids. J. Sound Vib. **320**, 1100–1130 (2009)
15. Falsone, G., Settineri, D.: A Kirchhoff-like solution for the Mindlin plate model: a new finite element approach. Mech. Res. Commun. **40**, 1–10 (2012)
16. Falsone, G., Settineri, D.: An Euler–Bernoulli-like finite element method for Timoshenko beams. Mech. Res. Commun. **38**, 12–16 (2011)
17. Stephen, N.G.: The second frequency spectrum of Timoshenko beams. J. Sound Vib. **80**, 578–582 (1982)
18. Stephen, N.G.: The second spectrum of Timoshenko beam theory—further assessment. J. Sound Vib. **292**, 372–389 (2006)
19. Stephen, N.G.: Mindlin plate theory: best shear coefficient and higher spectra validity. J. Sound Vib. **202**, 539–553 (1997)
20. Levinson, M.: Free vibrations of a simply supported, rectangular plate: an exact elasticity solution. J. Sound Vib. **98**, 289–298 (1998)
21. Elishakoff, I.: An equation both more consistent and simpler than the Bresse–Timoshenko equation. In: Gilat, R., Banks-Sills, L. (eds.) Advances in Mathematical Modeling and Experimental Methods for Materials and Structures, Solid Mechanics and Its Applications. Springer, Berlin, pp. 249–254 (2010)
22. Nesterenko, V.V.: A theory for transverse vibrations of a Timoshenko beam. PMM-J. Appl. Math. Mech. **57**, 669–677 (1993)
23. Timoshenko, S.P.: On the correction for shear of the differential equation for transverse vibration of prismatic bars. Philos. Mag. Ser. **6**(41), 744–746 (1921)
24. Elishakoff, I.: Generalization of the Bolotin's dynamic edge effect method for vibration analysis of Mindlin plates. In: Cuschieri, J.M., Glegg, S.A.L., Yeager, D.M. (eds.) National Conference on Noise Control Engineering. New York, pp. 911–916 (1994)
25. Kaplunov, J.D., Kossovich, L.Y., Nolde, E.V.: Dynamics of Thin Walled Elastic Bodies. Academic Press, San Diego (1998)
26. Reddy, J.N.: On locking free shear deformable beam elements. Comput. Methods Appl. Mech. Eng. **149**, 113–132 (1997)
27. Averill, R.C., Reddy, J.N.: An assessment of four-noded plate finite element based on a generalized third-order theory. Int. J. Numer. Methods Eng. **33**, 1553–1572 (1992)
28. Hashemi, S.H., Arsanjani, M.: Exact characteristic equations for some of classical boundary conditions of vibrating moderately thick rectangular plates. Int. J. Solids Struct. **42**, 819–853 (2005)
29. Roberts, D.B.: Formulas for Natural Frequency and Mode Shape. Van Nostrand Reinhold, New York (1979)